

DiffQ: UNIFIED PARAMETER INITIALIZATION FOR VARIATIONAL QUANTUM ALGORITHMS VIA DIFFUSION MODELS

Chi Zhang* Mengxin Zheng[†] Qian Lou[†] Fan Chen*

[†]University of Central Florida, FL, USA

*Indiana University, Bloomington, IN, USA

ABSTRACT

Variational Quantum Algorithms (VQAs) are widely used in the noisy intermediate-scale quantum (NISQ) era, but their trainability and performance depend critically on initialization parameters that shape the optimization landscape. Existing machine learning–based initializers achieve state-of-the-art results yet remain constrained to single-task domains and small datasets of only hundreds of samples. We address these limitations by reformulating VQA parameter initialization as a generative modeling problem and introducing DiffQ, a parameter initializer based on the Denoising Diffusion Probabilistic Model (DDPM). To support robust training and evaluation, we construct a dataset of 15,085 instances spanning three domains and five representative tasks. Experiments demonstrate that DiffQ surpasses baselines, reducing initial loss by up to 8.95 and convergence steps by up to 23.4%.

Index Terms— Variational Quantum Algorithms, Parameter Initialization, Denoising Diffusion Probabilistic Models

1. INTRODUCTION

Motivation. Variational Quantum Algorithms (VQAs) [1] have emerged as leading methods for the noisy intermediate-scale quantum (NISQ) era [2]. By combining limited quantum resources with classical optimizers, they reduce reliance on fault-tolerant devices while offering resilience to noise [1], low circuit complexity [3], and design flexibility [4]. VQAs have already demonstrated success in quantum physics, chemistry, and materials science [5–7]. Despite this promise, their scalability remains a central challenge: as system size increases, optimization landscapes flatten exponentially [8], leading to vanishing gradients and poor convergence. Parameter initialization has therefore become a critical strategy [9], reshaping the landscape to enhance trainability and mitigate suboptimal convergence. Recent deep learning–based initialization methods [10–13] define the state of the art, yet they remain task-specific, depend on limited datasets, and are typically validated in narrow settings, constraining their generalizability across diverse VQA applications.

Contributions. Inspired by recent advances in Denoising Diffusion Probabilistic Models (DDPMs) [14], a state-of-the-art class of generative machine learning methods [15–18], we reformulate VQA parameter initialization as a generative modeling task. Specifically, we encode optimized VQA

parameters into input tensors and train a DDPM to denoise corrupted versions of these tensors, conditioned on textual prompts describing the VQA task. Once trained, the model can transform random noise into high-quality parameter tensors guided by task descriptions, which are then used to initialize VQAs. This formulation leverages the strong generalization and flexibility of DDPMs to produce robust and transferable initializations. We further evaluate DiffQ on large-scale datasets, demonstrating improved performance and scalability compared with existing methods. The key contributions of this work are as follows:

- **Model Architecture.** We introduce DiffQ, a framework for VQA parameter initialization that integrates task- and guidance-specific encodings with a DDPM-based architecture to enhance trainability and enable cross-task generalization. We further outline its training and inference procedures, offering a systematic methodology for deployment across diverse VQA applications.
- **Dataset Construction.** We construct a VQA dataset of 15,085 instances spanning three domains and five tasks, surpassing prior works [10–13] that are limited to a single task and only hundreds of samples. The dataset serves as both the benchmark for this study and a public resource to advance future research on VQA parameter initialization.

Performance Evaluation. We evaluate DiffQ on the five constructed datasets, demonstrating substantial gains over existing methods, including reductions in initial loss of up to 8.95 and convergence steps by up to 23.4%.

2. DiffQ FRAMEWORK

In this section, we introduce the proposed DiffQ framework. We first describe the encoding of VQA circuit parameters and text-based prompt guidance into input tensors. We then present the DDPM-based model architecture for parameter initialization. Finally, we outline the training strategy and inference procedure of DiffQ.

2.1. VQA Circuit Parameter and Conditioning Encoding

VQA Circuit Parameter Encoding. Prior machine learning–based approaches [19, 20] represent quantum circuits as three-dimensional tensors: the first dimension indexes qubits, the second specifies gate placement along the circuit depth, and the third denotes the gate type. Due to page limits, we omit details and refer readers to [19, 20]. We adopt the same

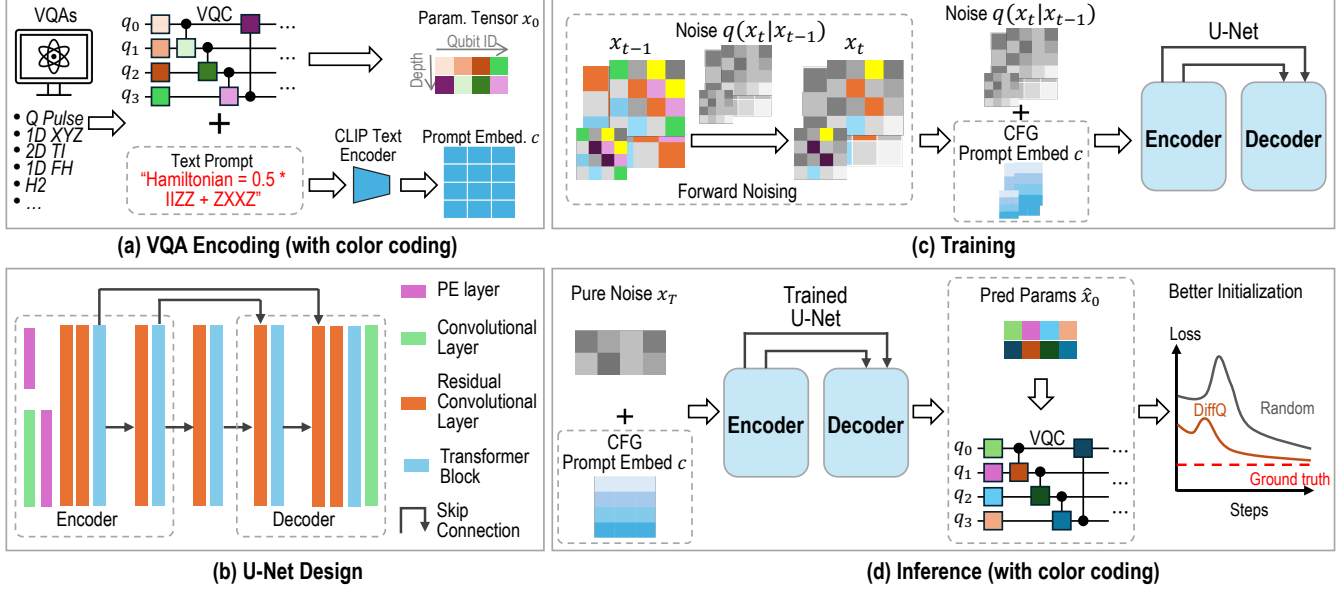


Fig. 1: The DiffQ framework: (a) encoding of VQA circuit parameters and text-based prompt guidance, (b) U-Net architecture for noise prediction, (c) training procedure of DiffQ, and (d) inference process of DiffQ.

representation but omit the third dimension, since the circuit ansatz is fixed for each task. This also enables a more compact depth dimension, as illustrated in Fig. 1(a). For instance, the two-qubit gate on q_0 need not appear at a later depth; all two-qubit gate parameters can be grouped together as long as the ansatz topology is known. This encoding provides a concise yet complete representation of circuit topology.

Conditioning Text Encoding. To guide parameter initialization across different VQAs, we use task-specific text prompts (Fig. 1(a)) that encode the defining features of each task. For example, in a variational quantum eigensolver (VQE) task, the prompt “Hamiltonian = $0.5 \cdot IIZZ + ZXXZ$ ” specifies the problem Hamiltonian, which uniquely characterizes the instance. The complete set of prompts for the five tasks studied in this work is given in Section 3 and summarized in Table 1. To convert these prompts into tensor representations suitable for conditioning a DDPM, we employ a pretrained CLIP encoder [21, 22], which aligns natural language with latent representations and enables text prompts to serve as effective conditioning inputs.

2.2. DiffQ Architecture

At a high level, DiffQ is formulated as a DDPM that progressively corrupts VQA parameter tensors in the training set with varying levels of Gaussian noise. The noise prediction network is trained to estimate this noise so that subtracting it from the corrupted input reconstructs the original clean tensors. For the prediction network, we adopt a U-Net backbone [23]. The U-Net employs an encoder–decoder structure with skip connections, which simultaneously preserves fine-grained spatial information and captures hierarchical features. To tailor this architecture for VQA parameter initialization, we extend the original convolution-only design with

several enhancements. First, sinusoidal positional encoding (PE) layers are introduced to embed the diffusion time step t , the noisy input tensor \mathbf{x}_t , and the conditioning text embedding \mathbf{c} , thereby incorporating temporal and contextual information into the generative process. Second, residual convolutional blocks [24] are integrated to improve feature extraction and training stability by facilitating gradient flow. Third, transformer blocks [25] are embedded within the architecture to capture long-range dependencies and enhance representational capacity beyond the locality of convolutional operations. The complete arrangement of these modules, including their depth and connectivity, is shown in Fig. 1(b).

2.3. Training and Inference of DiffQ

The training of DiffQ follows the standard Markov chain formulation of DDPMs, comprising a forward process that progressively corrupts data with Gaussian noise and a reverse process that reconstructs clean samples from noisy inputs.

Forward Process. The forward (noising) process incrementally perturbs data with Gaussian noise according to a variance schedule $\{\beta_t\}_{t=1}^T$:

$$q(\mathbf{x}_{1:T}|\mathbf{x}_0) = \prod_{t=1}^T q(\mathbf{x}_t|\mathbf{x}_{t-1}), \quad (1)$$

$$q(\mathbf{x}_t|\mathbf{x}_{t-1}) = \mathcal{N}(\mathbf{x}_t; \sqrt{1 - \beta_t} \mathbf{x}_{t-1}, \beta_t \mathbf{I}).$$

With $\alpha_t := 1 - \beta_t$ and $\bar{\alpha}_t := \prod_{s=1}^t \alpha_s$, the marginal distribution admits a closed form:

$$q(\mathbf{x}_t|\mathbf{x}_0) = \mathcal{N}(\mathbf{x}_t; \sqrt{\bar{\alpha}_t} \mathbf{x}_0, (1 - \bar{\alpha}_t) \mathbf{I}), \quad (2)$$

which enables direct sampling at any timestep. \mathbf{x}_0 denotes the optimized VQA parameters. As illustrated in Fig. 1(c), Gaussian noise is added batch-wise to parameter tensors, while prompt embeddings remain fixed. At each timestep t , the tensor \mathbf{x}_t is thus obtained by further corrupting \mathbf{x}_{t-1} .

Table 1: Dataset Overview

Application	Definition	Representative Prompt	# Parameters	# Qubits	# Instances
1D Heisenberg XYZ (1D_XYZ)	Equation (7)	" $(J_1, J_2, J_3) = (2, 1, 0.5)$ "	8	4	2000
1D Fermi–Hubbard Model (1D_FH)	Equation (8)	" $(t, U) = (0.5, 1)$ "	8	4	1000
2D Transverse-Field Ising Model (2D_TFI)	Equation (9)	" $(j, \mu) = (0.2, 3)$ "	16	8	1000
Quantum Pulse Synthesis (Q_Pulse)	cf. [26, 27]	" $h_0 = 0.3 ZI + 0.2 IZ; h_1 = 0.4 XI; U_t = e^{-iHt}$ "	24	2	8285
Random VQE	cf. [28]	"Hamiltonian = $0.5 \cdot IZZ + ZX XZ$ "	48	4	2800

Before feeding inputs into the model at timestep t , we apply classifier-free guidance (CFG) [29] to the prompt embeddings. Specifically, the text embedding \mathbf{c} is randomly mixed with a null embedding with probability p_{guidance} . This balances the trade-off between fidelity (matching the intended VQA description) and diversity (encouraging broader exploration of ansatz parameters) [18, 29].

Reverse Denoising Process. The reverse process is parameterized and learned. Starting from pure Gaussian noise $\mathbf{x}_T \sim \mathcal{N}(\mathbf{0}, \mathbf{I})$, the generative model is expressed as

$$p_\theta(\mathbf{x}_{0:T}) = p_\theta(\mathbf{x}_T) \prod_{t=1}^T p_\theta(\mathbf{x}_{t-1} | \mathbf{x}_t), \quad (3)$$

with Gaussian transitions of the form

$$p_\theta(\mathbf{x}_{t-1} | \mathbf{x}_t) = \mathcal{N}(\mathbf{x}_{t-1}; \mu_\theta(\mathbf{x}_t, t), \Sigma_\theta(\mathbf{x}_t, t)). \quad (4)$$

Here, θ denotes the parameters of the denoising network (the U-Net backbone), which predicts the conditional mean μ_θ and variance Σ_θ . At each timestep, the U-Net receives as input the noisy tensor \mathbf{x}_t , the timestep t , and the CFG-modified text embedding \mathbf{c} , and predicts the noise tensor $\hat{\epsilon}_\theta$. Sampling proceeds iteratively from $t = T$ to 0, generating a denoised parameter tensor \mathbf{x}_0 .

Training Loss. DiffQ parameters θ are optimized by minimizing the variational bound on the negative log-likelihood, which reduces to a denoising score-matching objective [30]:

$$L_{\text{MSE}} = \mathbb{E}_{\mathbf{x}_0, t, \epsilon} \left[\left\| \epsilon - \epsilon_\theta(\sqrt{\bar{\alpha}_t} \mathbf{x}_0 + \sqrt{1 - \bar{\alpha}_t} \epsilon, t) \right\|^2 \right], \quad (5)$$

where

$$\epsilon = \frac{\mathbf{x}_t - \sqrt{\bar{\alpha}_t} \mathbf{x}_0}{\sqrt{1 - \bar{\alpha}_t}}, \epsilon_\theta = \frac{\sqrt{1 - \bar{\alpha}_t}}{\beta_t} (\mathbf{x}_t - \sqrt{\bar{\alpha}_t} \mu_\theta(\mathbf{x}_t, t)). \quad (6)$$

In this formulation, $\epsilon_\theta(\cdot, t)$ is the neural network’s prediction of the noise added at timestep t . Once the prediction error between ϵ_θ and the true noise ϵ is minimized across all timesteps, the training of DiffQ is complete.

Inference. At inference time, given an unseen VQA task, the objective is to generate a parameter tensor \mathbf{x}_0 that provides a high-quality initialization for the corresponding VQA ansatz. As depicted in Fig. 1(d), the textual description of the task is first mapped to an embedding \mathbf{c} using the OpenCLIP encoder. Classifier-free guidance (CFG) is applied to \mathbf{c} to reinforce semantic alignment with the task description while retaining generative diversity. Initialization begins with a Gaussian noise tensor $\mathbf{x}_T \sim \mathcal{N}(\mathbf{0}, \mathbf{I})$, which is progressively denoised by the trained U-Net from timestep T to 0, conditioned on the embedding \mathbf{c} . The resulting tensor \mathbf{x}_0 is then decoded via the inverse of the circuit encoding scheme in Fig. 1(a) to recover the VQA ansatz parameters.

3. DATASET CONSTRUCTION

We construct comprehensive VQA datasets spanning three domains with five representative tasks, each paired with optimized ansatz parameters and a corresponding text prompt template capturing key task features. Each dataset comprises thousands of instances, in contrast to prior work [10–13], which typically provide only hundreds of samples. The first domain is *quantum many-body physics*, represented by three tasks: the Heisenberg XYZ model (1D_XYZ) with Hamiltonian in Eq. (7); the Fermi–Hubbard model (1D_FH) with Hamiltonian in Eq. (8); and the Transverse–Ising model (2D_TFI) with Hamiltonian in Eq. (9). Beyond many-body physics, we introduce two additional domains: *quantum pulse synthesis* (Q_Pulse), as described in [26, 27, 31–33], and *general random variational quantum eigensolvers* (VQE), detailed in [28]. Instances are generated by varying problem parameters, with circuits optimized using standard techniques in PennyLane and TorchQuantum [27]. Dataset statistics and key features are summarized in Table 1.

$$\hat{H} = \sum_{i=0}^3 (J_1 X_i X_{i+1} + J_2 Y_i Y_{i+1} + J_3 Z_i Z_{i+1}), \quad (7)$$

$$\hat{H} = -t \sum_{i=0}^{n-1} (\hat{c}_i^\dagger \hat{c}_{i+1} + \hat{c}_{i+1} \hat{c}_i) + U \sum_{i=0}^{n-1} \hat{n}_i \hat{n}_{i+1}, \quad (8)$$

$$\hat{H} = -j \sum_{i,j} Z_i Z_j - \mu \sum_i Z_i. \quad (9)$$

4. EXPERIMENTAL SETUP AND RESULTS

4.1. Experimental Setup

We conduct experiments to evaluate the performance of DiffQ on the constructed datasets. The evaluation metrics follow prior work [10–13], namely the average initial loss and the average number of convergence steps in VQA optimization. Since existing methods [10–13] are limited to a single application domain (e.g., many-body physics or quantum pulse synthesis), we adopt random initialization as a general baseline for comparison. For each application, all instances are randomly split into training and testing sets with a ratio of 7 : 3. We train DiffQ on each application independently and evaluate its performance on the corresponding test set. Unless otherwise specified, the diffusion step is set to $T = 100$, the guidance scale to $g = 10$, and the noise schedule to linear, ranging from $\beta_0 = 0.0001$ to $\beta_T = 0.02$. Each model is trained for 500 epochs with a maximum learning rate of 5×10^{-5} on a single NVIDIA RTX 3090 GPU.

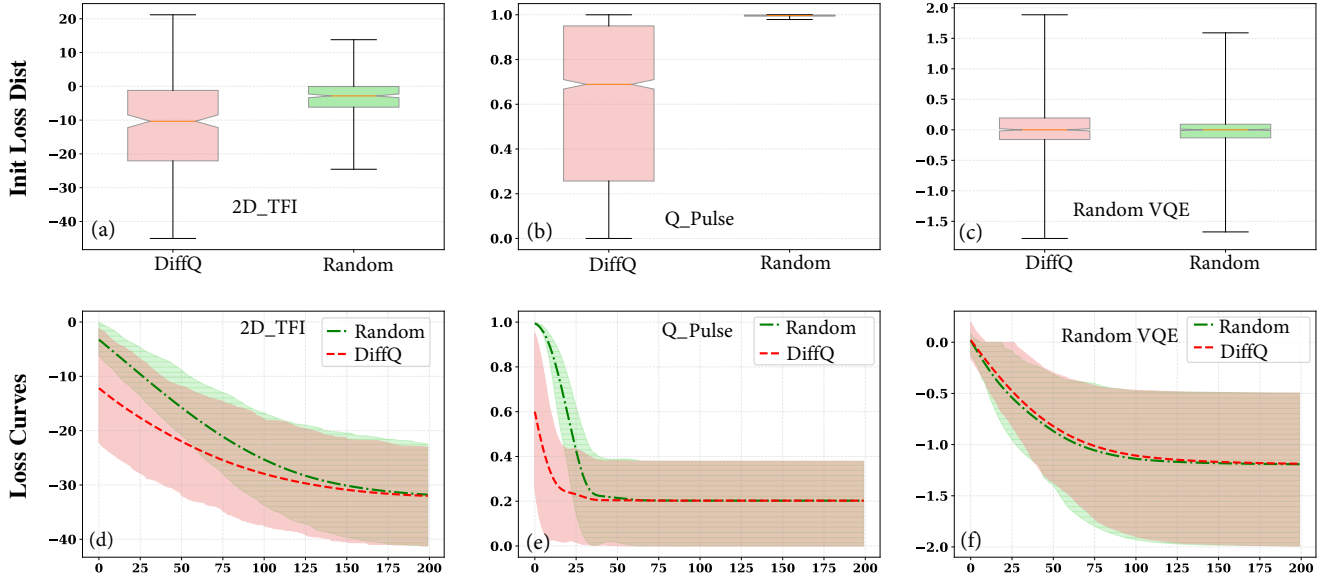


Fig. 2: Initial loss distributions and training loss trajectories for three distinct tasks.

Table 2: Comparison of DiffQ with random initialization. Δ denotes the relative difference, where positive values indicate improvement and negative values indicate degradation.

Applications	Schemes	Initial Loss	Convergence Steps
1D_XYZ	Random	0.06	266.93
	DiffQ	-0.16	251.89
	Δ	0.22 ↓	5.6% ↓
1D_FH	Random	1.01	218.46
	DiffQ	0.47	213.21
	Δ	0.54 ↓	2.4% ↓
2D_TFI	Random	-3.23	235.93
	DiffQ	-12.18	180.83
	Δ	8.95 ↓	23.4% ↓
Q_Pulse	Random	0.99	93.21
	DiffQ	0.60	81.98
	Δ	0.39 ↓	12% ↓
Random VQE	Random	0.02	237.82
	DiffQ	0.02	250.26
	Δ	0	5.2% ↑

4.2. Experimental Results

Overall Performance Comparison. Table 2 summarizes the performance of DiffQ relative to random initialization, evaluated in terms of initial loss and convergence steps across five datasets. All values are averaged over the corresponding test sets, with relative differences from random initialization highlighted in red. Overall, DiffQ consistently outperforms the baseline by achieving lower initial loss (with reductions of up to 8.95) and faster convergence (requiring up to 23.4% fewer optimization steps). These improvements are particularly significant for NISQ devices, where faster convergence reduces exposure to quantum noise and lowers computational cost. For the Random VQE tasks, however, DiffQ performs comparably to or slightly worse than random initialization. This limitation arises because such tasks lack meaningful physical correlations, thereby reducing the utility of learned parameter

priors. These observations indicate that DiffQ is most effective in settings where domain-specific structures are present, underscoring its relevance for realistic quantum applications that demand both scalability and precision.

Initial Loss and Convergence Analysis. Figure 2 further compares DiffQ with random initialization across three representative applications: 2D_TFI, Q_Pulse, and Random VQE. Figures 2(a–c) show the distributions of initial losses across all test instances, while Figures 2(d–f) depict the corresponding convergence trajectories. In the convergence plots, the shaded regions denote the range of losses across all instances, and the dashed curves represent pointwise averages.

For the 2D_TFI and Q_Pulse tasks, DiffQ achieves lower initial loss and faster convergence than random initialization. In the Q_Pulse case, random initialization causes degenerate behavior with losses collapsing near one, whereas DiffQ avoids this issue and accelerates convergence. By contrast, in the Random VQE task, DiffQ shows no clear advantage, as both initial loss and convergence closely match random initialization. This reflects the task’s simplicity (a single Pauli term), where learned priors are unnecessary. Overall, these results demonstrate that DiffQ is highly effective in structured, domain-informed applications but offers limited benefits for trivial or unstructured problems.

5. CONCLUSION

We present DiffQ, a unified framework for generating high-quality ansatz parameters in variational quantum algorithms. Based on a denoising diffusion probabilistic model, DiffQ iteratively transforms random noise into task-specific ansatz parameters conditioned on textual descriptions of the target problem. Experiments show that DiffQ consistently surpasses random initialization, achieving lower initial loss and faster convergence across diverse quantum applications.

6. REFERENCES

- [1] Marco Cerezo et al., “Variational quantum algorithms,” *Nature Reviews Physics*, vol. 3, no. 9, pp. 625–644, 2021.
- [2] Kishor Bharti et al., “Noisy intermediate-scale quantum algorithms,” *Reviews of Modern Physics*, vol. 94, no. 1, pp. 015004, 2022.
- [3] Yu Zhang et al., “Variational quantum eigensolver with reduced circuit complexity,” *npj Quantum Information*, vol. 8, no. 1, pp. 96, 2022.
- [4] Abhinav Kandala et al., “Hardware-efficient variational quantum eigensolver for small molecules and quantum magnets,” *nature*, vol. 549, no. 7671, pp. 242–246, 2017.
- [5] Bela Bauer et al., “Quantum algorithms for quantum chemistry and quantum materials science,” *Chemical reviews*, vol. 120, no. 22, pp. 12685–12717, 2020.
- [6] Yifan Li et al., “Variational quantum simulation for quantum chemistry,” *Advanced Theory and Simulations*, vol. 2, no. 4, pp. 1800182, 2019.
- [7] Jules Tilly et al., “The variational quantum eigensolver: a review of methods and best practices,” *Physics Reports*, vol. 986, pp. 1–128, 2022.
- [8] Jarrod R McClean et al., “Barren plateaus in quantum neural network training landscapes,” *Nature communications*, vol. 9, no. 1, pp. 4812, 2018.
- [9] Martin Larocca et al., “A review of barren plateaus in variational quantum computing,” *arXiv:2405.00781*, 2024.
- [10] Koen Mesman et al., “NN-AE-VQE: Neural network parameter prediction on autoencoded variational quantum eigensolvers,” *arXiv:2411.15667*, 2024.
- [11] Zhiding Liang et al., “Graph Learning for Parameter Prediction of Quantum Approximate Optimization Algorithm,” *arXiv:2403.03310*, Mar. 2024.
- [12] Fanxu Meng and Xiangzhen Zhou, “Parameter Generation of Quantum Approximate Optimization Algorithm with Diffusion Model,” *2407.12242*, , no. *arXiv:2407.12242*, 2024.
- [13] Junyong Lee et al., “Q-MAML: Quantum Model-Agnostic Meta-Learning for Variational Quantum Algorithms,” *arXiv:2501.05906*, Jan. 2025.
- [14] Jascha Sohl-Dickstein et al., “Deep unsupervised learning using nonequilibrium thermodynamics,” in *International conference on machine learning*. pmlr, 2015, pp. 2256–2265.
- [15] Robin Rombach et al., “High-resolution image synthesis with latent diffusion models,” in *Proceedings of the IEEE/CVF conference on computer vision and pattern recognition*, 2022, pp. 10684–10695.
- [16] Jonathan Ho et al., “Video Diffusion Models,” *Advances in Neural Information Processing Systems*, vol. 35, pp. 8633–8646, Dec. 2022.
- [17] Zhifeng Kong et al., “DiffWave: A Versatile Diffusion Model for Audio Synthesis,” *arXiv:2009.09761*, 2021.
- [18] Prafulla Dhariwal and Alex Nichol, “Diffusion Models Beat GANs on Image Synthesis,” *arXiv:2105.05233*, 2021.
- [19] Thomas Fösel et al., “Quantum circuit optimization with deep reinforcement learning,” *arXiv:2103.07585*, 2021.
- [20] Florian Furrutter, Gorka Muñoz-Gil, and Hans J. Briegel, “Quantum circuit synthesis with diffusion models,” *Nature Machine Intelligence*, vol. 6, no. 5, pp. 515–524, May 2024.
- [21] Alec Radford et al., “Learning Transferable Visual Models From Natural Language Supervision,” *arXiv:2103.00020*, 2021.
- [22] Gabriel Ilharco et al., “Openclip,” July 2021.
- [23] Olaf Ronneberger, Philipp Fischer, and Thomas Brox, “U-Net: Convolutional Networks for Biomedical Image Segmentation,” *arXiv:1505.04597*, 2015.
- [24] Chun-Fu Chen, Quanfu Fan, and Rameswar Panda, “CrossViT: Cross-Attention Multi-Scale Vision Transformer for Image Classification,” *arXiv:2103.14899*, Aug. 2021.
- [25] Ashish Vaswani et al., “Attention Is All You Need,” *arXiv:1706.03762*, Aug. 2023.
- [26] Zhiding Liang et al., “NAPA: Intermediate-level Variational Native-pulse Ansatz for Variational Quantum Algorithms,” *arXiv:2208.01215*, 2024.
- [27] Hanrui Wang et al., “QuantumNAS: Noise-Adaptive Search for Robust Quantum Circuits,” in *2022 IEEE International Symposium on High-Performance Computer Architecture (HPCA)*, Apr. 2022, pp. 692–708.
- [28] Ang Li, Samuel Stein, Sriram Krishnamoorthy, and James Ang, “QASMBench: A Low-Level Quantum Benchmark Suite for NISQ Evaluation and Simulation,” *ACM Transactions on Quantum Computing*, vol. 4, no. 2, pp. 10:1–10:26, Feb. 2023.
- [29] Jonathan Ho and Tim Salimans, “Classifier-Free Diffusion Guidance,” *arXiv:2207.12598*, 2022.
- [30] Jonathan Ho, Ajay Jain, and Pieter Abbeel, “Denoising Diffusion Probabilistic Models,” *arXiv:2006.11239*, 2020.
- [31] Guang Hao Low, Theodore J. Yoder, and Isaac L. Chuang, “Optimal arbitrarily accurate composite pulse sequences,” *Physical Review A*, vol. 89, no. 2, pp. 022341, Feb. 2014.
- [32] Kenneth R. Brown, Aram W. Harrow, and Isaac L. Chuang, “Arbitrarily accurate composite pulse sequences,” *Physical Review A*, vol. 70, no. 5, pp. 052318, Nov. 2004.
- [33] J. True Merrill and Kenneth R. Brown, “Progress in compensating pulse sequences for quantum computation,” *arXiv:1203.6392*, 2012.